Contents lists available at ScienceDirect

Bioactive Materials

In vivo performance of a rare earth free Mg–Zn–Ca alloy manufactured using twin roll casting for potential applications in the cranial and maxillofacial fixation devices

Matthew S. Dargusch [a,*], Nagasivamuni Balasubramani [a], Nan Yang [a], Sean Johnston [a], Yahia Ali [a], Gui Wang [a], Jeffrey Venezuela [a], Jiwon Carluccio [a], Cora Lau [b], Rachel Allavena [c], Daniel Liang [d], Karine Mardon [e], Qingsong Ye [f,g,**]

[a] Centre for Advanced Materials Processing and Manufacturing (AMPAM), School of Mechanical and Mining Engineering, The University of Queensland, Brisbane, QLD 4072, Australia
[b] The University of Queensland, Biological Resources, Brisbane, QLD, 4072, Australia
[c] School of Veterinary Science, The University of Queensland, Gatton, QLD, 4343, Australia
[d] Commonwealth Scientific and Industrial Research Organisation (CSIRO), Clayton, Melbourne, Australia
[e] Centre for Advanced Imaging, National Imaging Facility, The University of Queensland, St Lucia, Brisbane, QLD, 4072, Australia
[f] Centre of Regenerative Medicine, Renmin Hospital of Wuhan University, Wuhan University, Wuhan, Wuhan, 430060, China
[g] Skeletal Biology Research Centre, Department of Oral and Maxillofacial Surgery, Massachusetts General Hospital, Harvard School of Dental Medicine, Boston, MA, 02114, United States

ARTICLE INFO

ABSTRACT

A magnesium alloy containing essential, non-toxic, biodegradable elements such as Ca and Zn has been fabricated using a novel twin-roll casting process (TRC). Microstructure, mechanical properties, in vivo corrosion and biocompatibility have been assessed and compared to the properties of the rare earth (RE) element containing WE43 alloy. TRC Mg-0.5 wt% Zn- 0.5 wt% Ca exhibited fine grains with an average grain size ranging from 70 to 150 μm. Mechanical properties of a TRC Mg-0.5Zn-0.5Ca alloy showed an ultimate tensile strength of 220 MPa and ductility of 9.3%. The TRC Mg-0.5Zn-0.5Ca alloy showed a degradation rate of 0.51 ± 0.07 mm/y similar to that of the WE43 alloy (0.47 ± 0.09 mm/y) in the rat model after 1 week of implantation. By week 4 the biodegradation rates of both alloys studied were lowered and stabilized with fewer gas pockets around the implant. The histological analysis shows that both WE43 and TRC Mg-0.5Zn-0.5Ca alloy triggered comparable tissue healing responses at respective times of implantation. The presence of more organized scarring tissue around the TRC Mg-0.5Zn-0.5Ca alloys suggests that the biodegradation of the RE-free alloy may be more conducive to the tissue proliferation and remodelling process.

1. Introduction

Injuries in the maxillofacial and cranial regions are significant clinical problems [1]. Facial trauma has been found to account for approximately 45% of all trauma [2] and road accidents are one of the major causes for these injuries [3,4]. The predominant fracture sites are mandible, nasal bone, alveolar processes and zygomatic bones [4,5]. The treatment of maxillofacial injuries remains one of the important health problems in many countries [1,2,4–6]. Titanium alloys (Ti) are the most widely used implants to treat maxillofacial and cranial fractures (miniplates and mesh) [7–9], and have many clinical level applications as these alloys are bio-inert and have excellent mechanical strength, osseointegration [10] and bioactivity [8,11]. Reconstruction after surgical removal of tumors is an important application for metals in craniofacial implants [12].

However, complications may arise from permanent implants requiring second surgery for the removal of implants due to infection, loosening (stress shielding [13]), implant failure [2], increases in the

serum metal levels (soft tissue and blood cells) in the surrounding connective tissues [14], and local destruction of soft or hard tissues around the implant [15]. The removal of Ti implants is debatable, however, in certain cases the release of Ti particles causes fibrous encapsulation and chronic inflammation that requires implant removal in up to 40% of the cases [16,17]. These removals require complex surgeries, which also incur additional expense [2,14]. The removal of the implant due to failure (10–17%) mostly occurs within the first year [9].

Resorbable polymer-based implants are considered as an alternative to Ti implants [17,18]. A comparative study of biodegradable polymers and Ti implants has shown good biological responses for zygomatic implants with the similar occurrence of paresthesia, infection and less dehiscence [17]. The need for materials which (i) eliminate the need for a secondary surgery, (ii) reduce pain or irritation, and (iii) do not interference with the growth and development of oral maxillofacial bones (for children), are the main motivations for degradable implants development [19]. However, polymer implants have been associated with several adverse effects [16,19–21]. For instance, rapid hydrolysis causing inflammatory reactions [19] and pre-operative breakage/-damage of the screws or plates [20]. Other issues with the polymers include abscess formation during removal procedures [16], as well as concerns regarding the size/shape of the implant, and insufficient mechanical strength [13,19]. These observations have been further complicated by the lack of availability of adequate long-term data (>6 years) [20,21].

Opportunities for biodegradable metals in medical implant applications has resulted in intense research activity [22–26]. The use of magnesium (Mg), in particular, in the manufacture of biodegradable implants has attracted research interest for some years because magnesium displays low toxicity, rapid excretion, and numerous bioactive effects, including improved bone formation and protection against oxidative stresses while exhibiting high rates of degradation and absorption by the body avoiding the need for a second surgery [27–29]. Historically rare earth (REs) elements have been of particular interest as alloying elements in Mg alloys because of their role in improving the elevated temperature strength of the material for automotive and aerospace applications [30,31]. WE43 or alloys with similar composition have been the most widely investigated for medical implant applications [32–45] such as stents [46–49], orthopedic screw applications [50,51] and wires [32]. Screws and plates (mandible plates) of Mg alloys as cranial and maxillofacial implants have also been evaluated for degradation and biocompatibility in unalloyed Mg and AZ31 alloy (3 wt %Al-1wt.%Zn) [52] and WE43 alloys [53–55]. Despite their attractiveness from a high strength, availability and low impurity standpoint, the physiological impacts of REs have raised many unanswered questions about their long-term impact [56,57]. For instance, Y, Ce and La were found to have cytotoxic effects and reduced cell viability [57]. Although there were no direct observations reported for toxic effects when the degradation is within the daily allowable limit (RE < 4.2 mg day^{-1}), it was suggested that heavier RE elements should be limited or avoided whenever possible as they show a greater affinity for skeletal tissue, and thus a longer biological half-life [57].

Thus, an alternative approach is to design alloys with only biologically compatible elements consisting of Mg, Zn and Ca that participate in a broad range of metabolic processes [56] and have a higher maximum daily dosage compared to RE elements [57]. Binary alloys of Mg–Zn and Mg–Ca have been investigated primarily to understand the degradation performance and mechanical properties of these alloys. Mg–Ca alloys containing 0.5 to 10 wt% Ca [58] experienced rapid corrosion with an increase in Ca content and this causes extensive hydrogen evolution for alloys with calcium contents above 5 wt% Ca [59]. The corrosion rate can be related to the amount of the Mg_2Ca phase in the alloy [60,61], and modifying the microstructure using heat treatment and secondary processing methods improves their mechanical and degradation performance [62,63]. Similarly, binary Mg–Zn alloys have been explored as biodegradable alloys in the as-cast state [64,65], homogenized [65,66]

wrought [67–70] and powder metallurgical routes [71], as Zn possesses good solubility and enhances strength. In contrast to Mg–Ca, the Mg_xZn_y intermetallic phases in Mg–Zn alloys acts as cathodic sites within the Mg matrix, and they are responsible for accelerated degradation rates at higher Zn concentrations [64,65]. Thus, tailoring the composition of Zn and Ca to a lower level has led to the development of Mg–Zn–Ca alloys (ZX series) with low alloying elements as High-Strength Low-Alloy (HSLA) Mg alloys [72]. The ZX alloys containing <1 wt% of Zn and Ca provides slower degradation rates than higher Zn containing alloy due to the presence of ternary $Mg_6Zn_3Ca_2$ phase that was found to accelerate pitting corrosion [72]. Studies have also shown a slower degradation rate [72], higher bone mineralization [73] and osteogenic properties for bone repair [74]. One of the main challenges in ZX00 (Zn and Ca < 1.0 wt%) alloy is to achieve a combination of better mechanical strength and ductility [75–77]. Generally, after casting, homogenization heat treatment combined with extrusion (direct/indirect) [78,79], rolling process [76,77] and severe plastic deformation such as equal channel angular pressing [75] have been performed to refine the grain size and intermetallic phases to improve the mechanical properties. On the other hand, this series of processing stages can significantly increase the cost of manufacturing Mg alloys and they are time-consuming [80,81]. Therefore, the current study is focussed on fabricating higher strength materials using a twin rolling process (TRC) and investigating the potential of these TRC Mg–Zn–Ca alloys [80]. Strip roll casting has been proposed as a manufacturing process that can impart particular high strengths and ductility through a combination of rapid solidification and mechanical working [82–84]. Thin strips of 0.5–2.5 mm can be directly produced from the liquid alloy that is fed into the rollers that provide higher cooling rates for microstructure refinement and improved mechanical properties are reported for AZ31, AM60 and AZ91 alloys similar to commercial wrought alloys [80,81].

Thus, the present work investigates the microstructure refinement, mechanical properties, in vivo degradation and tissue response of Mg–Zn–Ca alloy fabricated by the TRC process. Results have shown that the TRC Mg-0.5Zn-0.5Ca alloys exhibited better mechanical properties, slower in vivo degradation and comparable healing responses compared to WE43.

2. Experimental procedure

2.1. Alloy preparation

The Mg-0.5 wt% Zn-0.5 wt% Ca alloy was melted in an electric furnace under a mixture of protective cover gases. The melt was then transferred to a horizontal twin-roll caster machine and fed into the gap between its two rotating rolls. With the extraction of the heat by the two rolls, the melt was solidified into near-net-shape Mg alloy sheet of 4.0 mm thickness at a near-rapid cooling rate when passing through the gap. This as-cast Mg alloy strip was heated to a temperature in the range of 340 °C–350 °C before rolling to 1 mm thick [80,81]. A standard RE containing Mg alloy WE43 (3.57%Y-2.16%Nd-0.42%Gd-0.48%Zr-Bal% Mg, all the percentages are in wt.%) was cast, solution heat treated at 525 °C and age hardened at 250 °C for 16hr. This alloy was used as a reference to evaluate the microstructure refinement, in vivo degradation, gas development and biocompatibility.

2.2. Microstructure and mechanical properties characterization

For microstructure analysis, the samples were cut then hot mounted in a conductive resin for mechanical grinding and finish polishing using Struers TegraPol 21 automatic polisher. Firstly, samples were ground in SiC abrasive papers (grit sizes starting from 600, 1200 and 4000 respectively) and then using micro suspensions of diamond and colloidal silica to obtain a scratch-free surface. The samples were then etched using picric-acetic acid containing solution and examined under a polarized light optical microscope (Leica-Polyvar microscope). Hitachi

TM3030 tabletop scanning electron microscope (SEM) with energy dispersive spectroscopy (EDS) detector was used for phase analysis at 15 keV. Electron backscatter diffraction (EBSD) mapping was performed at 20 keV using a step size of 0.15 μm on a JEOL-6610-SEM equipped with Oxford/HKL EBSD detector. The data were then processed using HKL Channel 5 acquisition software. Unetched samples were used for SEM-EDS and EBSD analysis. Tensile tests were carried using Instron 5584 universal testing machine for the TRC Mg–Zn–Ca and WE43 alloy according to ASTM standard E8 [26]. For each alloy, at least 3 to 4 samples were tested to assure consistency and repeatability of results.

2.3. Sample preparation and animal model for in vivo testing

TRC Mg–Zn–Ca alloy plates (15 mm × 6 mm × 3 mm) and cylindrical samples of WE43 alloy (Ø6 mm × 15 mm) were used for in vivo study. The sharp corners or edges from the machined samples were ground to prevent any undesired tissue responses due to physical irritation and these samples were cleaned, weighed and then stored in a desiccator.

The in vivo test involved implantation in a small animal model (Wistar rats). The rats were subjected to the standard ad libitum rodent diet, and were allowed to inhale isoflurane (2% in O_2) as anaesthesia prior to the implantation surgery. The rat's hair was shaved in the vicinity of the insertion area, i.e. at the upper back just behind the shoulder, and at the lower back just in front of the thigh. The exposed skin was swabbed with antiseptic and incised. The implant was inserted subcutaneously, with each rat receiving an implant at each of the insertion location. Subsequently, the incision was secured using sutures, and the rat given an injection of painkillers. For each alloy, twelve rats were divided into two sub-groups of six for evaluation at 1 and 4 weeks. All procedures conform to the requirements of the University of Queensland (UQ) Animal Ethics Committee (approval number MME/161/17), the Animal Care and Protection Act Qld, and the Australian Code of Practice for the Care and Use of Animals for Scientific Purposes.

2.4. Gas development and corrosion evaluation

After 1 and 4 weeks of implantation time, the rats were anaesthetized and examined under μ-CT (Inveon multimodality PET/CT imaging scanner) before euthanasia. The scan settings include an operating voltage of 80 kV, current of 500 μA, exposure time of 230 ms and an isotropic voxel size of 104.96 μm. The software Inveon Research Workplace 4.2 was used for initial assessment of the μCT images and conversion of raw scans to DICOM slices for further analysis. Quantitative volume and surface area measurements of the gas pockets surrounding the implants were obtained by manipulating DICOM slices using ImageJ software. Each implant and gas pocket were visually located within the subject, and the corresponding slices extracted. A region of interest (ROI) was identified and cropped which encapsulates the entire gas pocket on all slices. The cropped set of slices were then duplicated, to isolate the implant and gas separately by adjusting the image threshold to produce a binary image. The threshold was adjusted individually for each implant to capture the maximum amount of gas as observed visually; substantial image artifacts (bright and dark streaks) were unavoidable in several images due to the metal implants, resulting in the selection of a variance of thresholds for both the implant and the gas. The raw STL files were visually assessed and cleaned using the software Autodesk Meshmixer for the estimation of the volume of gas pockets.

The implants were extracted after euthanasia after 1 and 4 weeks for corrosion analysis. The corrosion rate of the explanted specimens was calculated using weight loss analysis following ASTM G1-03 to convert mass loss into a degradation rate in mm/year [56].

2.5. Histological analysis

Histopathology assessment of TRC Mg–Zn–Ca alloy and WE43 alloy was performed after 1 and 4 weeks of implantation by a board-certified and experienced veterinary anatomic pathologist. Standardized histology sections of the implant and sham surgical sites were assessed on Haematoxylin and Eosin (H&E) stained 4-μm routine paraffin-embedded formalin fixed tissue.

3. Results

3.1. Microstructure analysis

Fig. 1 shows the grain structure of the TRC Mg–Zn–Ca and heat treated WE43 alloy [56]. To have a better understanding, TRC microstructures were examined in three different orientations along the rolling direction as shown in Fig. 1(a–c). Variations in the grain size are noted in parallel (Fig. 1 (a)), transverse (Fig. 1 (b)) and normal to the rolling directions (Fig. 1 (c)). As seen from Fig. 1 (a), the majority of the grains are elongated parallel to the rolling direction with an average grain size of <150 μm. At the top surface where the rolling force was highest, the grains are smaller (equiaxed) and sub-grains are formed due to the plastic deformation. These grains are too small to be resolved by the optical microscope, EBSD technique was used to further investigate the deformed grains. Fig. 1(b) shows an equiaxed grain structure with an average grain size of 115 ± 77 μm. This structure was expected due to the orientation of the sample (transverse to the rolling direction) at which constant force was applied along the whole plane during the rolling process. Fig. 1 (c) shows the microstructure normal to the rolling direction with predominantly equiaxed grains (grain size of 71 ± 27 μm). Although there are differences noted in along within the sample cross-section, the grain size ranges from 70 to 150 μm. Fig. 1 (d) shows the grain structure of cast and heat treated WE43 alloy with an average grain size of ~158 μm. A better refinement was obtained with TRC process, as it possesses a significant advantage of combining casting and rolling in a single step producing excellent refinement than the WE43 alloy.

Fig. 2 (a and b) shows the low and high magnification backscattered electron (BSE) images of the TRC alloy observed in the parallel direction. The severely etched (dark) regions are due to the presence of recrystallized grains along the grain boundaries. Fig. 2 (b) displays the image of dendritic grains with second phases as bright white particles present within the interdendritic regions of a grain. Similar observations were noted along with the transverse and normal directions. Unlike a commercial as-cast alloy, the second phases are not seen as segregations, which is one of the significant attributes of the TRC process that combines the advantage of rapid solidification and deformation processing. From the Mg–Ca–Zn ternary phase diagram [85], this intermetallic phase have been identified as Mg_2Ca and/or $Ca_2Mg_6Zn_3$ at 1 wt% addition level of Ca and Zn. A recent study on Mg–1Ca–1Zn alloy reported that the eutectic formed intermetallic consist of three lamellar structured phases (α-Mg + Mg_2Ca + $Ca_2Mg_6Zn_3$) and concentrated along the grain boundaries [86]. Fig. 2 (c and d) shows the BSE images of heat-treated WE43 alloy. Grain boundaries are clearly visible along with the RE's precipitates that are present within grains and along the grain boundaries (bright white feature marked by arrows). These RE precipitates are well-known in the heat treated WE43 alloy that usually contains Y, Nd and Zr (1.3–6.5 at. % Zr, 2.9–8.9 at. % Nd and 0.3–2.6 at. % Y) [87].

Fig. 3 (a) shows an optical microscopy image of the severely deformed region with fine, recrystallized grains present along the grain boundaries of elongated grains. Fig. 3 (b and c) shows the EBSD grain orientation maps and angle along the rolling direction to study the recrystallization behaviour. The inverse pole figure (IPF) map in Fig. 3 (b and c) shows the grain structure of the severely deformed area. Two main characteristics can be seen from the map, in which most of the grains are preferentially oriented along the $[\bar{1}2\bar{1}0]$ direction. Secondly, the severe plastic deformation has led to the recrystallization of fine
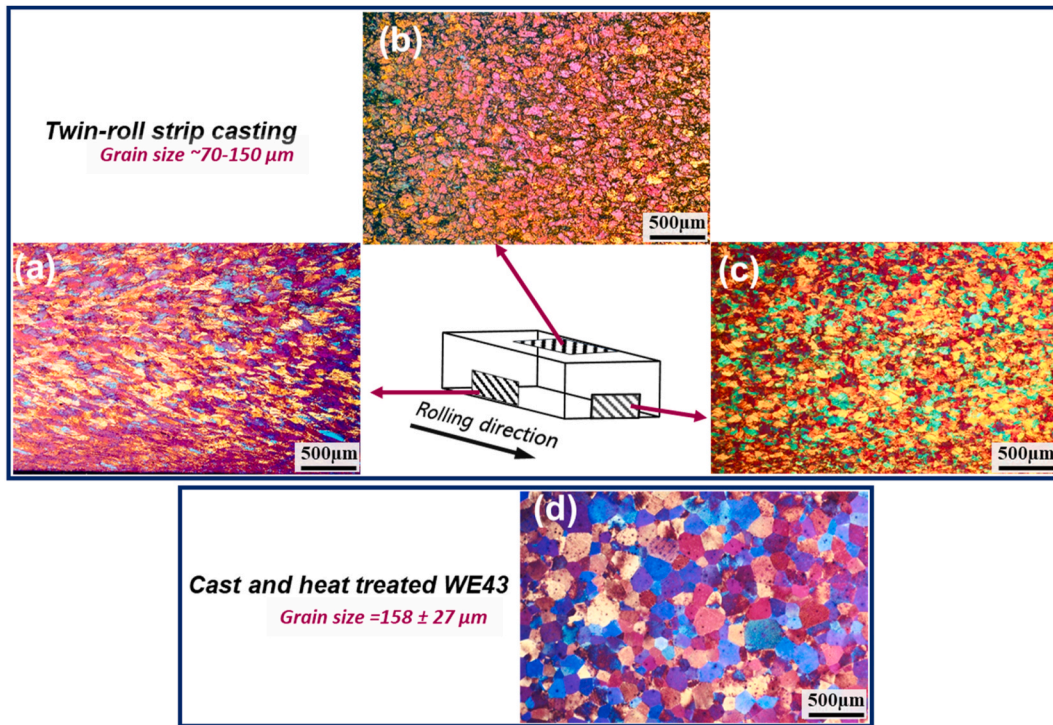
Fig. 1. Polarised light microscopic images of (a–c) TRC Mg–Zn–Ca alloy and (d) WE43 alloy [56].
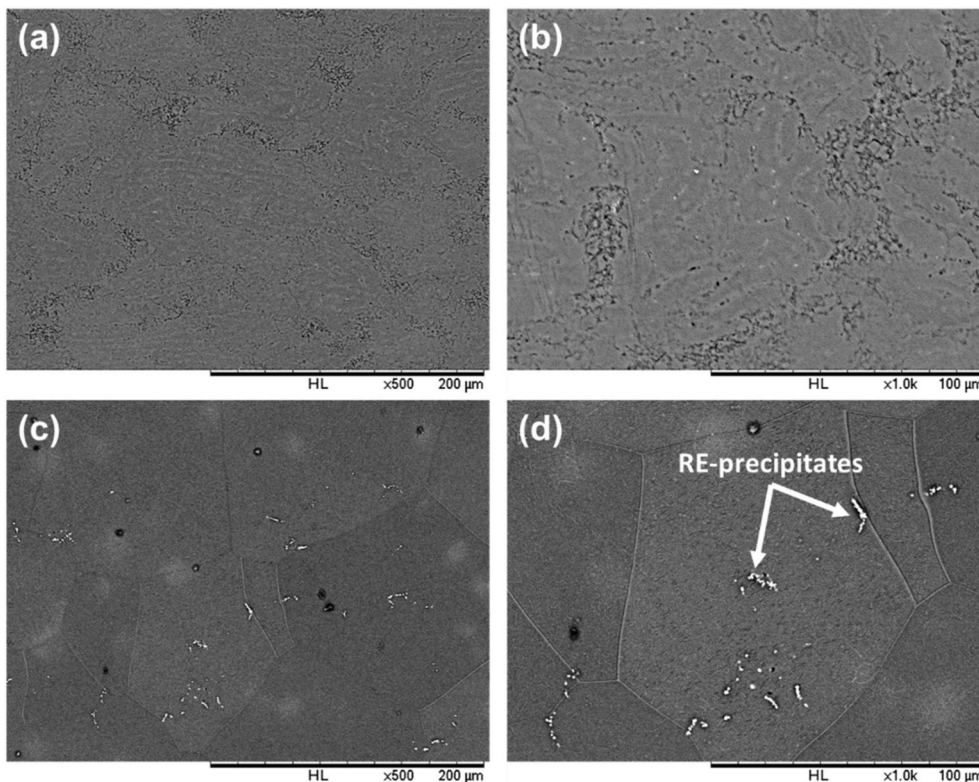

Fig. 2. Backscattered electron (BSE) images of (a, b) TRC Mg–Zn–Ca alloy and (c, d) WE43 alloy at (a, c) low and (b, d) high magnifications respectively.

grains along the boundaries of long columnar grains. This might be a result of the rolling process applying extensive force at the areas of close contact of the sample with the rollers. In addition, as shown in Fig. 3 (b₁ and c₁) rolling leads to strong texture in the metal that can be visualized from the orientation density function (ODF). Generally, ODF gives the density of grains having a particular orientation [88]. The misorientation angle distribution in Fig. 3 (b₂) shows that low energy boundaries (>15°) dominate the distribution, suggesting exposure of the grains to severe plastic deformation and dynamic recrystallization [89,90]. Another notable peak in the distribution is around 30°, which is
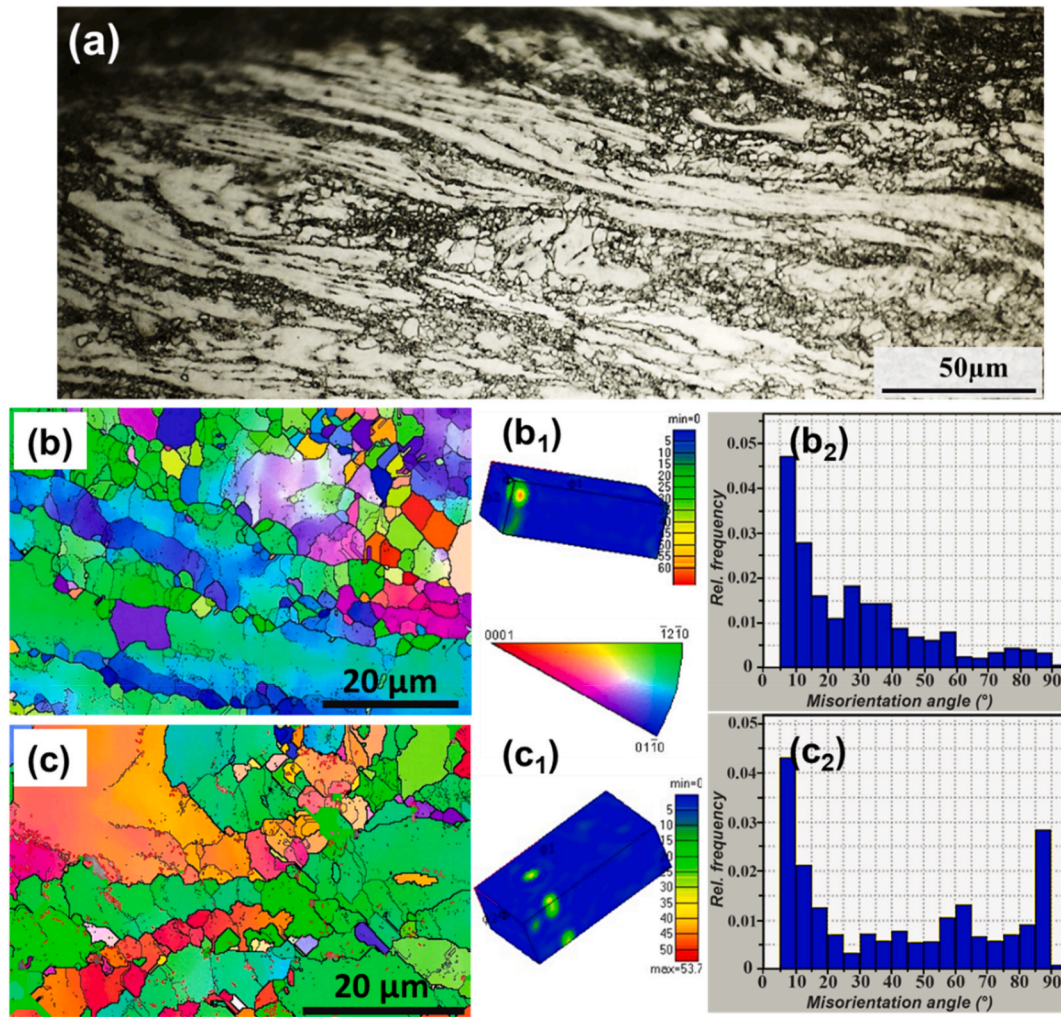
Fig. 3. (a) Bright-field optical image of the deformed region with recrystallized grains along the parallel direction. (b, c) Inverse pole figures at two random locations where (b_1, c_1) are the ODFs and (b_2, c_2) are the distribution of misorientation angles.

typically found for Mg sheets with strong texture [90]. The distribution in Fig. 3 (c_2) is different to that of the distribution shown in Fig. 3 (b_2). Not only that the low energy boundaries dominate the distribution, but peaks are observed around 85–90° and minor peaks are seen at 55°-65°. In the HCP system, these angles represent tensile, compression and

double twinning behaviour [90,91], which are expected to appear as a result of the rolling process. The distribution of fine grains observed from Fig. 3 (b and c) shows an average grain diameter less than 6 μm.
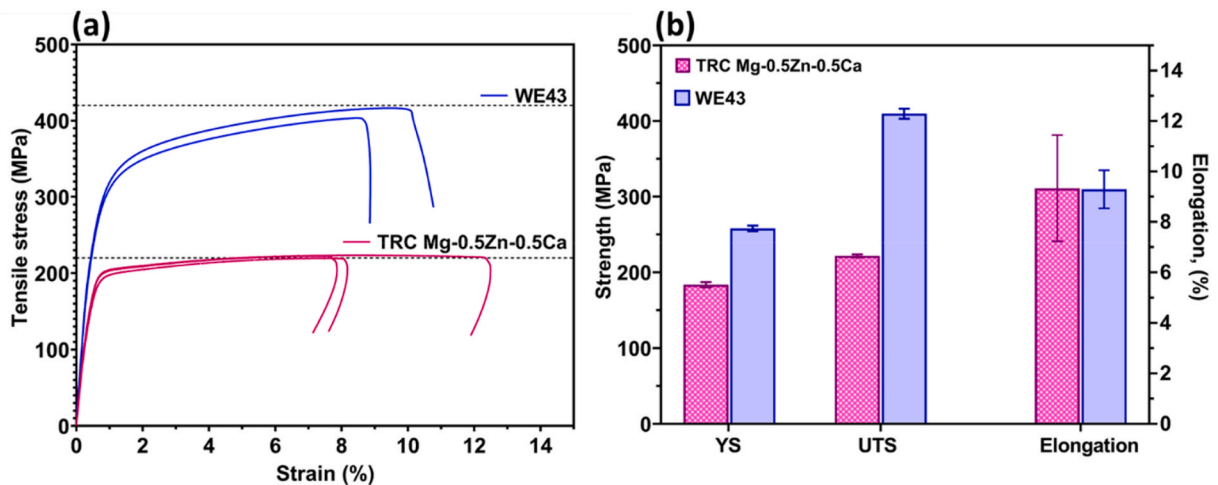

Fig. 4. (a) Tensile load curves and (b) summary of the mechanical properties of TRC Mg–Zn–Ca alloy and WE43 alloy.

3.2. Mechanical properties

Fig. 4 shows the tensile curves of TRC Mg–Zn–Ca alloy and WE43 alloy. For comparison, the derived tensile data is presented in Table 1. The results table shows the yield strength (YS), ultimate tensile strength (UTS) and elongation at failure (%). The TRC alloys showed an ultimate tensile strength of 221.9 ± 1.8 MPa and elongation of 9.3 ± 2.1%. The WE43 alloy has a higher yield strength (x 1.4) and ultimate tensile strength (x 1.9) compared to the TRC Mg–Zn–Ca alloy. However, the elongation values observed for Mg–Zn–Ca and WE43 alloy are comparable.

Table 2 shows the maximum tensile strength achieved for Mg–Zn–Ca series alloys reported in the literature and the processing methods adopted. Generally, the as-cast alloys show inferior strength and ductility due to coarse or dendritic grains and fully divorced eutectic structure. Commercial processing routes include homogenization heat treatment, rolling and extrusion processes [76,78,92,93]. Repeated annealing combined with deformation is a common approach to obtain the desired strength and indeed, it is challenging to improve the ductility and strength of the alloy simultaneously [92]. A relatively high Zn/Ca ratio has been found to increase the strength of the alloy; however, such compositions are associated with reduced ductility. Some alloys show exception, for instance, Mg–6Zn-1.5Ca achieved a UTS of 250 MPa and 14.7% elongation [79]. On the other hand, similar strength and ductility were reported for Mg-0.96Zn-0.29Ca with a UTS of 265 MPa and 31% elongation after indirection extrusion at 300 °C [78]. Comparing the results of the present work with the literature (Table 2), it is clear that the TRC alloy (fabricated into thin strips in a single step) exhibited a series of promising mechanical properties. This is reasonable for a RE free alloy that contains a significantly lower number of alloying elements compared to a WE43 alloy. Although the exact mechanical strength required of implants and devices used in maxillofacial surgery is difficult to determine, it is expected that many spacer-type applications require relatively low strength values (Gareb et al., [13]). During tissue healing processes, the load will be shared by the underlying bone and osteosynthesis system. It should be noted that having a higher strength is not always beneficial as it might cause stress shielding and implant resorption [13]. A higher strength and stiffness of magnesium alloys over biodegradable polymers is an advantage, however, controlling the degradation rate is the key to utilize the potential of lower strength TRC Mg–Zn–Ca alloy compared to WE43 alloy.

3.3. In vivo corrosion behaviour

Fig. 5 shows the in vivo degradation of TRC Mg–Zn–Ca and WE43 alloy after 1- and 4-week observation periods. In general, the degradation rate after 1 week in all these alloys is higher than that after 4 weeks of testing. The slower degradation associated with the 4 weeks samples is due to the formation of a protective layer (hydroxides, calcium phosphates and MgO) and the growth of fibroblastic reaction in the tissues in the region surrounding the implant [28,95,96]. A comparable degradation performance is noted for the TRC Mg–Zn–Ca alloy similar to that of the WE43 alloy, which is promising for the development of RE free Mg alloys.

Fig. 6 (a - d) presents the representative 3D reconstructed images

Table 1

Mechanical properties of twin-roll strip cast Mg–Zn–Ca alloy and the WE43 alloy.

Alloys	Yield strength (MPa)	Ultimate tensile strength (MPa)	Elongation (%)
TRC Mg-0.5Zn-0.5Ca	186.76	222.79	7.65
	185.45	223.63	12.31
	178.88	219.32	8.05
WE43	254.35	403.11	8.54
	261.66	416.22	10.05

Table 2

Mechanical properties of Mg–Zn–Ca alloys by different processing methods.

| Alloy composition (wt.%)	Zn/Ca ratio	Processing routes	Mechanical properties		Ref
			Tensile strength (MPa)	Elongation (%)	
Mg-1.0Zn-1.0Ca	1.0	Cast (C) → Homogenized (400 °C, 24h) → hot rolled (HR, 300 °C, 4.2 mm thickness) → heat treated (HT)	250 ± 6[HR]	4.0 ± 0.8	[76]
			222 ± 6[HT]	14.9 ± 1.6	
			201 ± 15[HT]	6.1 ± 1.8	
Mg-0.94Zn-0.15Ca	6.26	Cast → Homogenized (400 °C, 12h)	127 ± 2.1	7.5 ± 0.4	[92]
Mg-0.92Zn-1.54Ca	0.59		65 ± 1.1	1.5 ± 1.1	
Mg-2.72Zn-0.16Ca	17		141 ± 2.3	7.6 ± 0.4	
Mg-2.78Zn-1.65Ca	1.68		76 ± 1.2	0.4 ± 0.02	
Mg-4.67Zn-0.19Ca	24.57		145 ± 2.4	5.3 ± 0.3	
Mg-4.02Zn-1.41Ca	2.85		103 ± 1.7	1.4 ± 0.1	
		Cast → Homogenized (400 °C, 12h) → hot rolled (400 °C)	226 ± 3.7	4.1 ± 0.2	
			108 ± 1.8	0.4 ± 0.002	
			204 ± 3.3	1.3 ± 0.1	
			96 ± 1.6	0.2 ± 0.01	
			142 ± 2.3	0.9 ± 0.04	
			77 ± 1.3	0.2 ± 0.01	
Mg-0.96Zn-0.29Ca	3.31	300°C-Indirect extrusion	265	31	[78]
		325°C-Indirect extrusion	240	32	
		325°C-Direct extrusion	268	20	
		400°C- Direct extrusion Cast → Homogenized (350 °C, 12h) and solutionized (450 °C, 8h) → Extruded using direct and indirect methods (325 °C, 375 °C, 400 °C)	226	25	
Mg-6.0Zn-1.5Ca	4	Cast → Homogenized (350 °C, 12h) → Extruded (E, 300 °C) and annealed (EA, 350 °C, 1h)	120[C]	1.2	[79]
			332[E]	8.6	
			250[EA]	14.7	
Mg-0.6Zn-0.2Ca	3.0	Cast	120	6.0	[94]
Mg-2.0Zn-0.2Ca	10.0		178	6.5	
Mg-2.5Zn-0.2Ca	12.5		130	3.8	
Mg-3.0Zn-0.2Ca	15.0	Cast → Homogenized (380 °C, 24h) → Extruded (E, 300 °C, 1.0 mm plates) and annealed (300 °C, 2h)	270[E]	11.4	[93]
			234[A]	17.85	
Mg-0.5Zn-0.5Ca	1.0	Twin roll cast (TRC) and subsequently rolled (~340–350 °C, 1 mm thick plates)	221.9 ± 1.8	9.3 ± 2.1	This work
WE43	–	Cast and Heat treated	409.6 ± 6.5	9.3 ± 0.75	
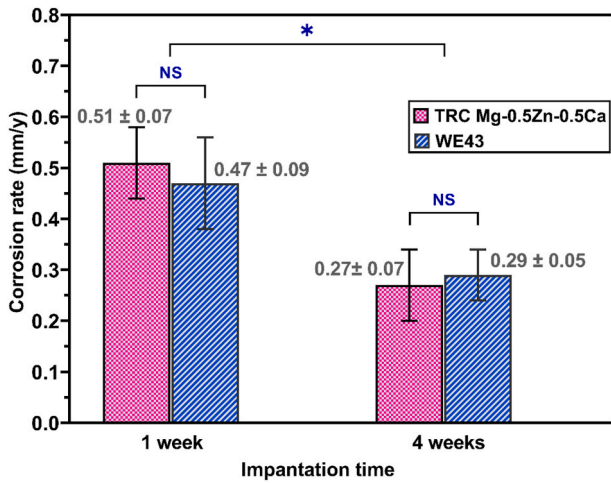
Fig. 5. In vivo corrosion rate of TRC Mg–Zn–Ca and WE43 alloys after 1 week and 4 weeks of implantation (asterisk represent statistical significance: *p < 0.05 and NS represent no significance).

showing the gas development behaviour of the TRC Mg–Zn–Ca, WE43 alloy after 1 and 4 weeks of implantation. Both WE43 and TRC Mg–Zn–Ca alloys produced clinically visible subcutaneous gas pockets within 1 week of implantation. The gas pockets are primarily located adjacent to the implant, as a result of the Mg degradation upon contact with the physiological environment [97]. Fig. 6(e–h) presents the

distribution of the gas pockets after 1 and 4 weeks of implantation of TRC Mg–Zn–Ca and WE43 alloys. In general, the TRC Mg–Zn–Ca group showed the highest value at 278.87 ± 112.01 mm^3 compared to the WE43 group (152.09 ± 81.15 mm^3). Larger values of standard deviation in the histograms of Fig. 6 (e and g) suggest that the gas pocket sizes of each implant group are scattered, likely due to the variables introduced during the implantation and 3D reconstruction process. Intriguingly, the distribution of the gas pocket size indicated a generally positive correlation to the degradation rate of the implants.

After 4 weeks of implantation, the size of the gas pockets was reduced to below 250 mm^3 in the majority of the implanted rats (Fig. 6 (f, h)) with an average size of 233.71 ± 408.25 mm^3 and 84.98 ± 113.74 mm^3 for TRC Mg–Zn–Ca and WE43 group, respectively. This is due to a reduction in the volume of gas generated as Mg corrosion slowed over this period. As for the pre-existing hydrogen gas, it has been proposed that the gas can escape via an exchange mechanism through the surrounding tissue [98], subsequently reducing the overall size of the pocket. This exchange mechanism would also be responsible for a change in the composition of the gas in the pocket. The remaining hydrogen gas saturates the surrounding tissues, and is continuously exchanged with other dissolved gases present in the blood stream (e.g., N_2, O_2, CO_2). Eventually, the exchanged gases take up the gas cavity, resulting in a mixture of H_2, N_2, O_2, CO and CO_2 [98–100] at 4 weeks, which are considered biologically safe to the implanted animals.

Although the development of the gas pocket is a commonly reported phenomenon during the in vivo degradation of Mg-based implant [101–103], it is worth noting that some samples of the TRC Mg–Zn–Ca alloy experienced an uncontrolled gas development. This is evident in
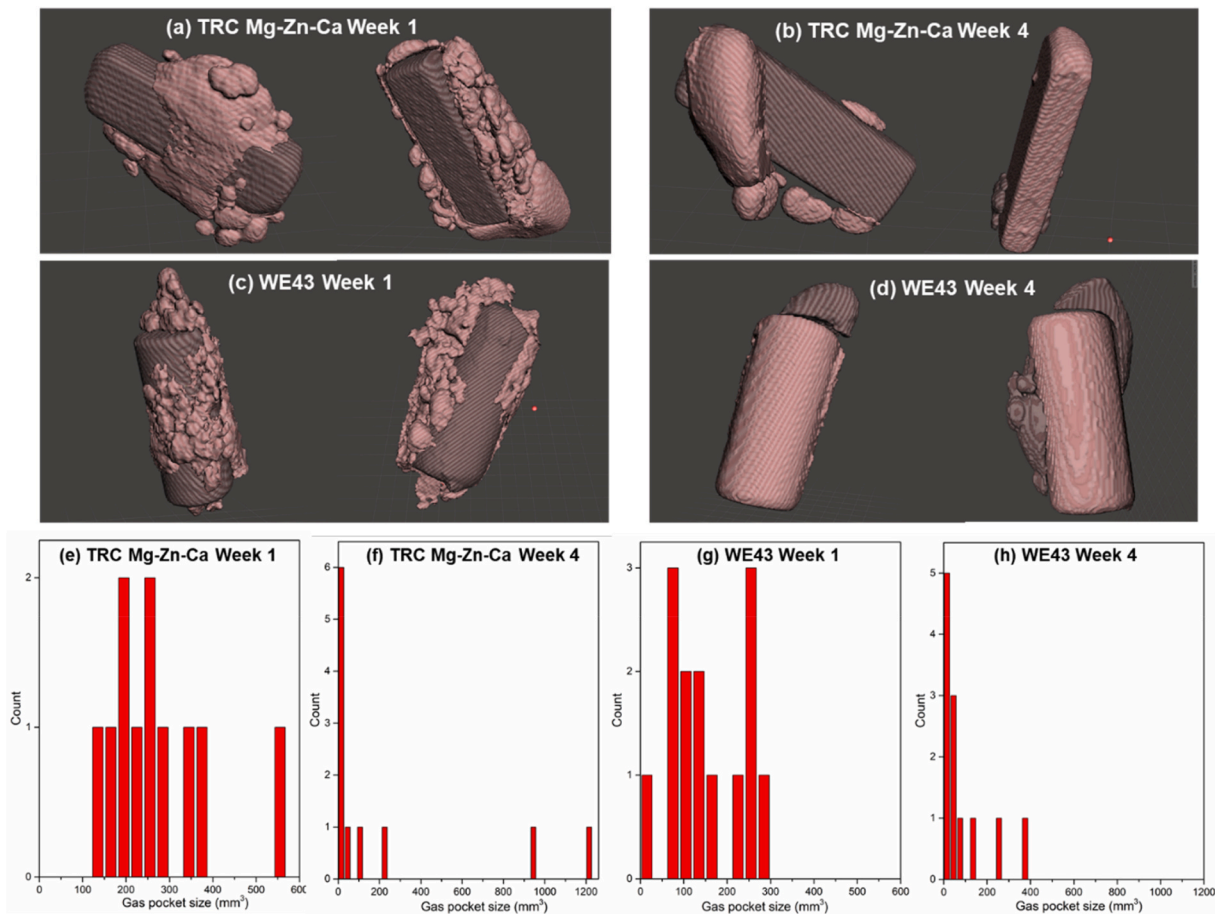

Fig. 6. Representative 3D reconstructed μ-CT images showing the presence of gas around (a, b) TRC Mg–Zn–Ca and (c, d) WE43 implant within rat model after 1 week and 4 weeks. (e, h) Histograms of the gas pocket size in (e, f) TRC Mg–Zn–Ca alloy and (g, h) WE43 alloy implant group after 1 week and 4 weeks of implantation.

Fig. 6 where some pocket sizes fell outside the first standard deviation limit. Uncontrolled gas pocket build-up could lead to complications such as wound dehiscence, bone defects, or reducing the implant's radiopacity [104]. Although all animals survived and tolerated the implantation period in the current study, the reasons for the excessive gas build up in some implantation groups are worth investigating.

3.4. In vivo biocompatibility

Fig. 7 presents the H&E-stained histological appearance of the TRC Mg–Zn–Ca and WE 43 implanted tissues after 1 and 4 weeks of implantation. According to Fig. 7 (a and b), both implanted materials triggered active fibroplasia and leukocytic responses after 1 week, consistent with response to implantation of a foreign material. The tissue around the TRC Mg–Zn–Ca implant indicated severe fibroplasia reaction with the evident build-up of loosely connected extracellular collagen; the inner tissue layer adjacent to the implant location is infiltered with 1–3 cell layers of macrophages, suggesting moderate leukocytic response to a foreign body (Fig. 7 (a)). The WE43 implanted tissue showed a high level of tissue reactivity with macrophages and multinucleated giant cells present at the lining of the tissue-implant interface, indicating foreign body reaction. After 4 weeks, both scarring and inflammatory responses started to settle at the implantation sites (Fig. 7 (c and d)). As shown in Fig. 7 (c), the dense, organized fibrous tissue is formed around the TRC Mg–Zn–Ca implant, with the capsule wall thickness of 100–250 μm. Occasional macrophages can be found at the inner edge of the capsule, indicating mild residual leukocytic response. The tissue around the WE43 implant indicated a similar inflammatory response compared to that of the TRC Mg–Zn–Ca implant group, and scar tissue starting to become more organized by 4 weeks.

Healthy animals exhibit acute inflammatory and fibroplasia responses upon the implantation of biomaterials, with leukocytic cells, typically macrophages or multi-nucleate giant cells derived from macrophages, infiltrating into the implanted tissue then attempting to coat and ingest the foreign bodies [105]. Therefore, the increased level of macrophage infiltration at the implantation sites in both groups is expected and consistent with the foreign body responses to biomaterials. After 4 weeks, the leukocytic responses in both implant groups were significantly reduced, and the fibroplasia reaction was progressing to an organized capsule. Overall, both implanted materials are considered to be bio-safe to the host tissue as they neither resulted in significant tissue necrosis nor negatively interfered with the tissue healing and encapsulation responses. It is particularly interesting to note that the fibrous tissue around the TRC Mg-0.5Zn-0.5Ca implanted group became more organized after 4 weeks compared to the WE43 implanted group. It is likely that the RE-free alloy may promote the tissue proliferation and remodelling process, although the exact mechanism is yet to be determined.

4. Discussion

Twin roll casting of Mg alloys is an effective approach for the production of high-performance Mg alloys [80,81], specifically to promote refined microstructure for low alloying element containing Mg–Zn–Ca alloys (Fig. 1(a–c)). In a typical RE containing WE43 alloy the presence of Zr and RE elements promote grain refinement during solidification (Fig. 1(d)) and precipitation strengthening effect when heat treated. For the solute-lean Mg-0.5Zn-0.5Ca alloy (only 1 wt% of total alloying element), conventional slow cooling conditions would result in large and dendritic grains [56]. One of the key issues of having higher Zn or Ca contents is that these elements, on one hand, promote refinement and strength, while, on the other hand, the corrosion rate can be accelerated by undissolved Ca-rich binary or ternary secondary intermetallic phases [86]. The thermally stable Ca-rich intermetallic phases can be expected to act as galvanic sites for localized corrosion even after rolling or extrusion processes [92]. With the total alloying concentration is below 1 wt%, no segregation was identified in TRC Mg–Zn–Ca alloys (Fig. 2 (a and b)). Several recrystallized grains were found on the rolled surface that exhibit a strong texture along the rolling direction, however, the remaining regions with equiaxed grains exhibit superior mechanical properties and elongation (Fig. 4).

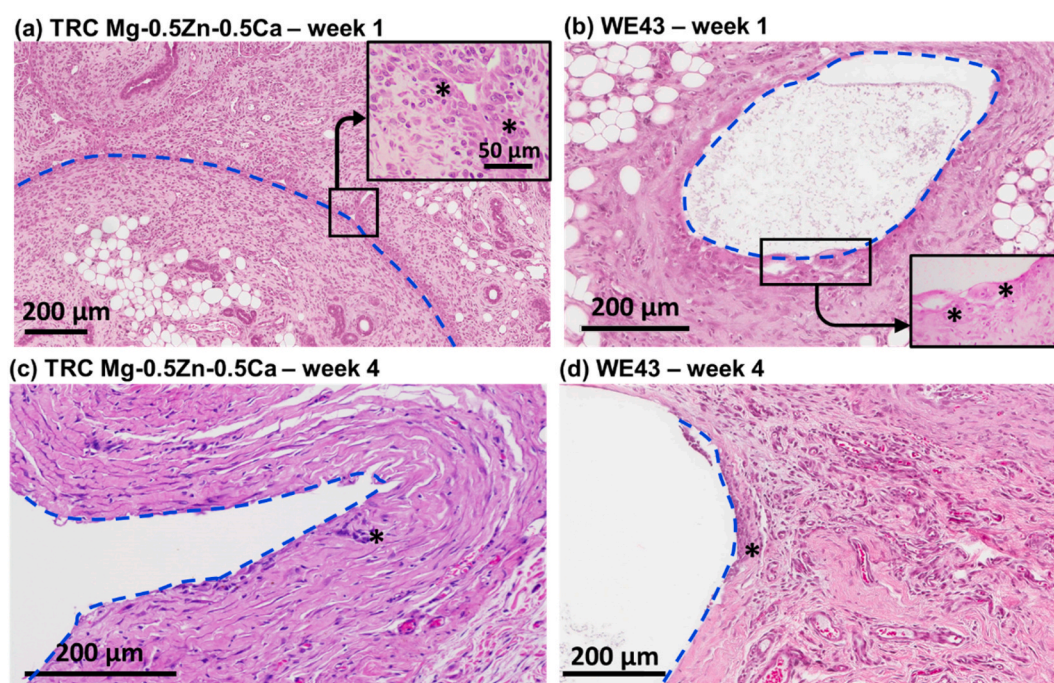Cranial/Maxillofacial fixation devices are used in a complex

Fig. 7. Histological appearance of the H&E stained tissue after (a, b) 1 week and (c, d) 4 weeks of in vivo testing. The inserted images in (a) and (b) show macrophages lining the pocket wall for TRC Mg-0.5Zn-0.5Ca alloy and multinucleate giant cells and macrophages for WE43 alloy respectively (indicated by *). Dashed lines indicate the tissue in direct contact with the implant.

physiological environment, where the screws penetrate through bones (hard tissue), and the plates are placed at the bone-tissue interface (soft tissue) [53]. While the responses to the hard tissue environment have been widely studied for Mg alloys [52–55], the soft tissue responses and the early stages of degradation or the gas development are less studied. In a maxillofacial/oral environment, the gas development and soft tissue responses including inflammatory and fibroplasia responses could affect both short term and long-term cosmetic appearance of the surgical site of the patient. For instance, it is worth noting that that few studies have shown the potential of using Mg–Zn–Ca alloys as vascular clips [106, 107] and these clips are in oral/maxillofacial surgery to get a better access to the surgical site in some cases. Currently, many fixtures used in maxillofacial and mandibular applications uses plates (or miniplates) with a locking screw arrangement that are made from bioinert Ti alloys. Recently, several Mg alloys including unalloyed Mg, AZ31 [52], WE43 [53–55] and Mg–Zn–Ca alloys [73] have been tested in vivo as craniofacial screws and plates. In general, all these alloys exhibit new bone formation, no sign of inflammation or adverse effects to the soft tissue adjacent to the implant or the degradation product and these alloys also promote bone healing. Among these Mg based alloys, Mg–Zn–Ca alloy shown particularly attractive characteristics as bone implant materials for the promotion osteogenesis [108] and antimicrobial properties [109]. As the degrading implant generate Mg^{2+} as corrosion product, Mg^{2+} could up-regulate the osteoblastic activity of osteoblasts by activating the signal pathways to promote the proliferation and osteogenic differentiation [110,111]. One of the limitations of Mg–Zn–Ca alloys is the relatively low strength compared to the main alternative, WE43 alloy. This study has shown that Mg–Zn–Ca samples produced using Twin Roll Casting have much higher strengths than similar alloys produced using more conventional methods due to the uniform and fine grain structure characteristics of the process. The development of gas around the implant has been reported to occur at the initial stages of implantation for Mg–Zn–Ca alloys [73], which is similar to the observations reported in the current work. However, a significant reduction in gas pocket size was noted after a 4-week implantation period. The current study has the limitation of being a short duration study in the subcutaneous region of a rat model, primarily focussed on understanding the initial degradation behaviour and tissue response of the Mg–Zn–Ca alloy fabricated through TRC process. Further studies are required to examine the degradation and biocompatibility of actual components fabricated using TRC Mg–Zn–Ca alloys such as miniplates inserted within appropriate animal models.

5. Conclusions

Magnesium alloys containing minor addition of Ca and Zn (0.5 wt%) have been fabricated using a twin roll casting process (TRC, a single step casting and rolling process) and tested in vivo for degradation, gas development and biocompatibility. The important observations of this study can be summarized as follows.

(1) The TRC Mg-0.5Zn-0.5Ca alloy showed excellent refinement with grain sizes less than 150 μm and exhibited an ultimate tensile strength and elongation of 221.9 ± 1.8 MPa and 9.3 ± 2.1% respectively.

(2) A comparable in vivo degradation rate was observed for the TRC Mg-0.5Zn-0.5Ca and WE43 alloy after 1 and 4 weeks of in vivo testing. Initially, a rapid degradation was noted after one week (0.51 ± 0.07 mm/y for TRC Mg–Zn–Ca alloy vs 0.47 ± 0.09 mm/y for WE43 alloy) and the rate of degradation was lowered after 4 weeks (0.27 ± 0.07 for TRC Mg–Zn–Ca alloy vs 0.29 ± 0.09 mm/y for WE43 alloy).

(3) Large gas pockets surrounding the implants were noted after 1 week of implantation and the size distribution of gas pockets was relatively larger for Mg–Zn–Ca alloy than WE43 alloy. After 4 weeks of implantation, a significant reduction was observed in

the gas pockets. However, it should be noted that large deviations exist in the size distribution even after 4 weeks in both the alloys, suggesting the influence of additional factors and this requires further study.

(4) Histological analysis indicated that both WE43 and TRC Mg-0.5Zn-0.5Ca alloy triggered tissue leukocytic and fibroblastic responses. TRC Mg–Zn–Ca alloys showed a promising healing response due to the presence of organized scar tissue, which is beneficial for tissue remodelling process. Results from this preliminary study show that Mg–Zn–Ca alloys could be promising implants for RE free, maxillofacial fixation devices.

CRediT authorship contribution statement

Matthew S. Dargusch: Conceptualization, Methodology, Investigation, Data curation, for alloy fabrication and microstructure characterization, Methodology, Investigation, Data curation, and Analysis of in vivo experiments, Formal analysis, Validation, Writing – original draft, Writing – review & editing, Supervision, Resources and Funding acquisition. **Nagasivamuni Balasubramani:** Methodology, Investigation, Data curation, for alloy fabrication and microstructure characterization, Formal analysis, Validation, Writing – original draft. **Nan Yang:** Methodology, Investigation, Data curation, and Analysis of in vivo experiments. Formal analysis, Validation, Writing – original draft. **Sean Johnston:** Methodology, Investigation, Data curation, and Analysis of in vivo experiments. **Yahia Ali:** Methodology, Investigation, Data curation, for alloy fabrication and microstructure characterization. **Gui Wang:** Methodology, Investigation, Data curation, for alloy fabrication and microstructure characterization. **Jeffrey Venezuela:** Methodology, Investigation, Data curation, and Analysis of in vivo experiments. **Jiwon Carluccio:** Methodology, Investigation, Data curation, and Analysis of in vivo experiments. **Cora Lau:** Methodology, Investigation, Data curation, and Analysis of in vivo experiments. **Rachel Allavena:** Methodology, Investigation, Data curation, and Analysis of in vivo experiments. **Daniel Liang:** Methodology, Investigation, Data curation, for alloy fabrication and microstructure characterization. **Karine Mardon:** Methodology, Investigation, Data curation, and Analysis of in vivo experiments. **Qingsong Ye:** Conceptualization, Writing – review & editing, Supervision.

Declaration of competing interest

The authors declare that they have no known competing financial interests or personal relationships that could have appeared to influence the work reported in this paper.

Acknowledgements

References

[1] U. Klammert, U. Gbureck, E. Vorndran, J. Rödiger, P. Meyer-Marcotty, A. C. Kübler, 3D powder printed calcium phosphate implants for reconstruction of cranial and maxillofacial defects, J. Cranio-Maxillo-Fac. Surg. 38 (2010) 565–570, https://doi.org/10.1016/j.jcms.2010.01.009.

[2] Y. Yu, W. Liu, J. Chen, L. Quan, X. Zheng, L. Liu, No need to routinely remove titanium implants for maxillofacial fractures, J. Oral Maxillofac. Surg. 77 (2019) 783–788, https://doi.org/10.1016/j.joms.2018.10.022.

[3] A. Ogunbowale, L. Costello, D. McCormack, K. Ekanayake, G.J. Kearns, Maxillofacial fractures in females: a 5-year retrospective review, Ir. J. Med. Sci. (2021), https://doi.org/10.1007/s11845-021-02534-1.

[4] M.A. Jaber, F. AlQahtani, K. Bishawi, S.T. Kuriadom, Patterns of maxillofacial injuries in the Middle East and North Africa: a systematic review, Int. Dent. J. (2021), https://doi.org/10.1111/idj.12587.

[5] M.H.S.S. Patoway, S. Ab Rahman, M. Wan Ahmed, T. Liszen, R. Shaari, Correlation among the fractured facial bones in a teaching hospital in Malaysia: a retrospective study of recent 5-years, J. Oral Maxillofac. Surg. Med. Pathol. 32 (2020) 14–18, https://doi.org/10.1016/j.ajoms.2019.10.014.

[6] A. Mijiti, W. Ling, M. Tuerdi, A. Maimaiti, J. Tuerxun, Y.Z. Tao, A. Saimaiti, A. Moming, Epidemiological analysis of maxillofacial fractures treated at a university hospital, Xinjiang, China: a 5-year retrospective study, J. Cranio-Maxillo-Fac. Surg. 42 (2014) 227–233, https://doi.org/10.1016/j.jcms.2013.05.005.

[7] J. Acero, J. Calderon, J.I. Salmeron, J.J. Verdaguer, C. Concejo, M. L. Somacarrera, The behaviour of titanium as a biomaterial: microscopy study of plates and surrounding tissues in facial osteosynthesis, J. Cranio-Maxillo-Fac. Surg. 27 (1999) 117–123, https://doi.org/10.1016/S1010-5182(99)80025-0.

[8] J. Kwarcinski, P. Boughton, A. Ruys, A. Doolan, J. van Gelder, Cranioplasty and craniofacial reconstruction: a review of implant material, manufacturing method and infection risk, Appl. Sci. 7 (2017), https://doi.org/10.3390/app7030276.

[9] H. Llandro, R. Langford, Reasons for plate removal after treatment of orbitozygomatic complex fractures, J. Cranio-Maxillo-Fac. Surg. 43 (2015) 17–20, https://doi.org/10.1016/j.jcms.2014.10.003.

[10] J. Yang, Y.S. Zhang, P. Lei, X. Hu, M. Wang, H. Liu, X. Shen, K. Li, Z. Huang, J. Huang, J. Ju, Y. Hu, A. Khademhosseini, "Steel–Concrete" inspired biofunctional layered hybrid cage for spine fusion and segmental bone reconstruction, ACS Biomater. Sci. Eng. 3 (2017) 637–647, https://doi.org/10.1021/acsbiomaterials.6b00666.

[11] A. Palmquist, O.M. Omar, M. Esposito, J. Lausmaa, P. Thomsen, Titanium oral implants: surface characteristics, interface biology and clinical outcome, J. R. Soc. Interface 7 (2010) S515–S527, https://doi.org/10.1098/rsif.2010.0118.focus.

[12] B. Tan, Q. Tang, Y. Zhong, Y. Wei, L. He, Y. Wu, J. Wu, J. Liao, Biomaterial-based strategies for maxillofacial tumour therapy and bone defect regeneration, Int. J. Oral Sci. 13 (2021) 9, https://doi.org/10.1038/s41368-021-00113-9.

[13] B. Gareb, C.C. Roossien, N.B. van Bakelen, G.J. Verkerke, A. Vissink, R.R.M. Bos, B. van Minnen, Comparison of the mechanical properties of biodegradable and titanium osteosynthesis systems used in oral and maxillofacial surgery, Sci. Rep. 10 (2020) 18143, https://doi.org/10.1038/s41598-020-75299-9.

[14] L.G. Mercuri, M. Miloro, A.K. Skipor, D. Bijukumar, C. Sukotjo, M.T. Mathew, Serum metal levels in maxillofacial reconstructive surgery patients: a pilot study, J. Oral Maxillofac. Surg. 76 (2018) 2074–2080, https://doi.org/10.1016/j.joms.2018.04.014.

[15] G.D. Wood, Inion biodegradable plates: the first century, Br. J. Oral Maxillofac. Surg. 44 (2006) 38–41, https://doi.org/10.1016/j.bjoms.2005.07.026.

[16] N.B. van Bakelen, G.J. Buijs, J. Jansma, J.G.A.M. de Visscher, T.J.M. Hoppenreijs, J.E. Bergsma, B. Stegenga, R.R.M. Bos, Comparison of biodegradable and titanium fixation systems in maxillofacial surgery:A two-year multi-center randomized controlled trial, J. Dent. Res. 92 (2013) 1100–1105, https://doi.org/10.1177/0022034513508953.

[17] B.C.L. da Silva, D. Souto-Souza, G.M. de Souza, R.A. Magesty, B. de Cassia Ávila, E.L. Galvão, S.G.M. Falci, Comparison between resorbable plates vs. titanium plates for treatment of zygomatic fractures: a systematic review with meta-analysis, Oral Maxillofac. Surg. (2021), https://doi.org/10.1007/s10006-020-00937-5.

[18] G.J. Buijs, N.B. van Bakelen, J. Jansma, J.G.A.M. de Visscher, T.J.M. Hoppenreijs, J.E. Bergsma, B. Stegenga, R.R.M. Bos, A randomized clinical trial of biodegradable and titanium fixation systems in maxillofacial surgery, J. Dent. Res. 91 (2012) 299–304, https://doi.org/10.1177/0022034511434353.

[19] G. Wittwer, W.L. Adeyemo, K. Yerit, M. Voracek, D. Turhani, F. Watzinger, G. Enislidis, Complications after zygoma fracture fixation: is there a difference between biodegradable materials and how do they compare with titanium osteosynthesis? Oral Surg. Oral Med. Oral Pathol. Oral Radiol. Endod. 101 (2006) 419–425, https://doi.org/10.1016/j.tripleo.2005.07.026.

[20] B. Gareb, N.B. van Bakelen, P.U. Dijkstra, A. Vissink, R.R.M. Bos, B. van Minnen, Biodegradable versus titanium osteosynthesis in maxillofacial traumatology: a systematic review with meta-analysis and trial sequential analysis, Int. J. Oral Maxillofac. Surg. 49 (2020) 914–931, https://doi.org/10.1016/j.ijom.2019.11.009.

[21] O.M. Böstman, H.K. Pihlajamäki, Adverse tissue reactions to bioabsorbable fixation devices, Clin. Orthop. Relat. Res. 371 (2000).

[22] F. Kiani, C. Wen, Y. Li, Prospects and strategies for magnesium alloys as biodegradable implants from crystalline to bulk metallic glasses and composites—a review, Acta Biomater. 103 (2020) 1–23, https://doi.org/10.1016/j.actbio.2019.12.023.

[23] H. Li, J. Wen, Y. Liu, J. He, H. Shi, P. Tian, Progress in research on biodegradable magnesium alloys: a review, Adv. Eng. Mater. 22 (2020) 2000213, https://doi.org/10.1002/adem.202000213.

[24] J. Venezuela, M.S. Dargusch, The influence of alloying and fabrication techniques on the mechanical properties, biodegradability and biocompatibility of zinc: a comprehensive review, Acta Biomater. 87 (2019) 1–40, https://doi.org/10.1016/j.actbio.2019.01.035.

[25] J.J.D. Venezuela, S. Johnston, M.S. Dargusch, The prospects for biodegradable zinc in wound closure applications, Adv. Healthc. Mater. 8 (2019) 1900408, https://doi.org/10.1002/adhm.201900408.

[26] N. Yang, N. Balasubramani, J. Venezuela, S. Almathami, C. Wen, M. Dargusch, The influence of Ca and Cu additions on the microstructure, mechanical and degradation properties of Zn–Ca–Cu alloys for absorbable wound closure device

[27] J.-L. Wang, J.-K. Xu, C. Hopkins, D.H.-K. Chow, L. Qin, Biodegradable magnesium-based implants in orthopedics—a general review and perspectives, Adv. Sci. 7 (2020) 1902443, https://doi.org/10.1002/advs.201902443.

[28] Y. Chen, J. Dou, H. Yu, C. Chen, Degradable magnesium-based alloys for biomedical applications: the role of critical alloying elements, J. Biomater. Appl. 33 (2019) 1348–1372, https://doi.org/10.1177/0885328219834656.

[29] U. Riaz, I. Shabib, W. Haider, The current trends of Mg alloys in biomedical applications—a review, J. Biomed. Mater. Res. B Appl. Biomater. 107 (2019) 1970–1996, https://doi.org/10.1002/jbm.b.34290.

[30] S. Tekumalla, S. Seetharaman, A. Almajid, M. Gupta, Mechanical properties of magnesium-rare earth alloy systems: a review, Metals-Basel 5 (2015) 1–39, https://doi.org/10.3390/met5010001.

[31] A.A. Luo, Recent magnesium alloy development for elevated temperature applications, Int. Mater. Rev. 49 (2004) 13–30, https://doi.org/10.1179/095066004225010497.

[32] K. Chen, Y. Lu, H. Tang, Y. Gao, F. Zhao, X. Gu, Y. Fan, Effect of strain on degradation behaviors of WE43, Fe and Zn wires, Acta Biomater. 113 (2020) 627–645, https://doi.org/10.1016/j.actbio.2020.06.028.

[33] X. Zhang, G. Yuan, L. Mao, J. Niu, W. Ding, Biocorrosion properties of as-extruded Mg–Nd–Zn–Zr alloy compared with commercial AZ31 and WE43 alloys, Mater. Lett. 66 (2012) 209–211, https://doi.org/10.1016/j.matlet.2011.08.079.

[34] S. Wang, Z. Han, Y. Nie, J. Dai, X. Li, J. Cheng, X. Zhang, Modified mechanical properties of Mg-Nd-Zn-Ag-Zr alloy by solution treatment for cardiovascular stent application, Mater. Res. Express 6 (2019), 085416, https://doi.org/10.1088/2053-1591/ab27ee.

[35] D. Liu, D. Yang, X. Li, S. Hu, Mechanical properties, corrosion resistance and biocompatibilities of degradable Mg-RE alloys: a review, J. Mater. Res. Technol. 8 (2019) 1538–1549, https://doi.org/10.1016/j.jmrt.2018.08.003.

[36] J. Wang, H. Zhou, L. Wang, S. Zhu, S. Guan, Microstructure, mechanical properties and deformation mechanisms of an as-cast Mg–Zn–Y–Nd–Zr alloy for stent applications, J. Mater. Sci. Technol. 35 (2019) 1211–1217, https://doi.org/10.1016/j.jmst.2019.01.007.

[37] A.C. Hänzi, I. Gerber, M. Schinhammer, J.F. Löffler, P.J. Uggowitzer, On the in vitro and in vivo degradation performance and biological response of new biodegradable Mg–Y–Zn alloys, Acta Biomater. 6 (2010) 1824–1833, https://doi.org/10.1016/j.actbio.2009.10.008.

[38] Q. Wu, S. Zhu, L. Wang, Q. Liu, G. Yue, J. Wang, S. Guan, The microstructure and properties of cyclic extrusion compression treated Mg–Zn–Y–Nd alloy for vascular stent application, J. Mech. Behav. Biomed. Mater. 8 (2012) 1–7, https://doi.org/10.1016/j.jmbbm.2011.12.011.

[39] M. Li, F. Benn, T. Derra, N. Kröger, M. Zinser, R. Smeets, J.M. Molina-Aldareguia, A. Kopp, J. Llorca, Microstructure, mechanical properties, corrosion resistance and cytocompatibility of WE43 Mg alloy scaffolds fabricated by laser powder bed fusion for biomedical applications, Mater. Sci. Eng. C 119 (2021) 111623, https://doi.org/10.1016/j.msec.2020.111623.

[40] Y. Li, H. Jahr, X.Y. Zhang, M.A. Leeflang, W. Li, B. Pouran, F.D. Tichelaar, H. Weinans, J. Zhou, A.A. Zadpoor, Biodegradation-affected fatigue behavior of additively manufactured porous magnesium, Addit. Manuf. 28 (2019) 299–311, https://doi.org/10.1016/j.addma.2019.05.013.

[41] H. Windhagen, K. Radtke, A. Weizbauer, J. Diekmann, Y. Noll, U. Kreimeyer, R. Schavan, C. Stukenborg-Colsman, H. Waizy, Biodegradable magnesium-based screw clinically equivalent to titanium screw in hallux valgus surgery: short term results of the first prospective, randomized, controlled clinical pilot study, Biomed. Eng. Online 12 (2013) 62, https://doi.org/10.1186/1475-925X-12-62.

[42] H. Waizy, J. Diekmann, A. Weizbauer, J. Reifenrath, I. Bartsch, V. Neubert, R. Schavan, H. Windhagen, In vivo study of a biodegradable orthopedic screw (MgYREZr-alloy) in a rabbit model for up to 12 months, J. Biomater. Appl. 28 (2014) 667–675, https://doi.org/10.1177/0885328212472215.

[43] A. Kopp, T. Derra, M. Müther, L. Jauer, J.H. Schleifenbaum, M. Voshage, O. Jung, R. Smeets, N. Kröger, Influence of design and postprocessing parameters on the degradation behavior and mechanical properties of additively manufactured magnesium scaffolds, Acta Biomater. 98 (2019) 23–35, https://doi.org/10.1016/j.actbio.2019.04.012.

[44] Y. Li, J. Zhou, P. Pavanram, M.A. Leeflang, L.I. Fockaert, B. Pouran, N. Tümer, K. U. Schröder, J.M.C. Mol, H. Weinans, H. Jahr, A.A. Zadpoor, Additively manufactured biodegradable porous magnesium, Acta Biomater. 67 (2018) 378–392, https://doi.org/10.1016/j.actbio.2017.12.008.

[45] L. Mao, L. shen, J. Chen, X. Zhang, M. Kwak, Y. Wu, R. Fan, L. Zhang, J. Pei, G. Yuan, C. Song, J. Ge, W. Ding, A promising biodegradable magnesium alloy suitable for clinical vascular stent application, Sci. Rep. 7 (2017) 46343, https://doi.org/10.1038/srep46343.

[46] C.M. Campos, T. Muramatsu, J. Iqbal, Y.-J. Zhang, Y. Onuma, H.M. Garcia-Garcia, M. Haude, P.A. Lemos, B. Warnack, P.W. Serruys, Bioresorbable drug-eluting magnesium-alloy scaffold for treatment of coronary artery disease, Int. J. Mol. Sci. 14 (2013) 24492–24500, https://doi.org/10.3390/ijms141224492.

[47] G. Mani, M.D. Feldman, D. Patel, C.M. Agrawal, Coronary stents: a materials perspective, Biomaterials 28 (2007) 1689–1710, https://doi.org/10.1016/j.biomaterials.2006.11.042.

[48] C. DI Mario, H. Griffiths, O. Goktekin, N. Peeters, J. Verbist, M. Bosiers, K. Deloose, B. Heublein, R. Rohde, V. Kasese, C. Ilsley, R. Erbel, Drug-Eluting bioabsorbable magnesium stent, J. Intervent. Cardiol. 17 (2004) 391–395, https://doi.org/10.1111/j.1540-8183.2004.04081.x.

[49] D. Schranz, P. Zartner, I. Michel-Behnke, H. Akintürk, Bioabsorbable metal stents for percutaneous treatment of critical recoarctation of the aorta in a newborn,

Cathet. Cardiovasc. Interv. 67 (2006) 671–673, https://doi.org/10.1002/ccd.20756.

[50] J.-M. Seitz, A. Lucas, M. Kirschner, Magnesium-based compression screws: a novelty in the clinical use of implants, JOM 68 (2016) 1177–1182.

[51] J.L. Niu, M.P. Xiong, X.M. Guan, J. Zhang, H. Huang, J. Pei, G.Y. Yuan, The in vivo degradation and bone-implant interface of Mg-Nd-Zn-Zr alloy screws: 18 months post-operation results, Corrosion Sci. 113 (2016) 183–187, https://doi.org/10.1016/j.corsci.2016.10.009.

[52] S.E. Henderson, K. Verdelis, S. Maiti, S. Pal, W.L. Chung, D.-T. Chou, P.N. Kumta, A.J. Almarza, Magnesium alloys as a biomaterial for degradable craniofacial screws, Acta Biomater. 10 (2014) 2323–2332, https://doi.org/10.1016/j.actbio.2013.12.040.

[53] B. Schaller, N. Saulacic, T. Imwinkelried, S. Beck, E.W.Y. Liu, J. Gralla, K. Nakahara, W. Hofstetter, T. Iizuka, In vivo degradation of magnesium plate/screw osteosynthesis implant systems: soft and hard tissue response in a calvarial model in miniature pigs, J. Cranio-Maxillo-Fac. Surg. 44 (2016) 309–317, https://doi.org/10.1016/j.jcms.2015.12.009.

[54] H. Naujokat, J.-M. Seitz, Y. Açil, T. Damm, I. Möller, A. Gülses, J. Wiltfang, Osteosynthesis of a cranio-osteoplasty with a biodegradable magnesium plate system in miniature pigs, Acta Biomater. 62 (2017) 434–445, https://doi.org/10.1016/j.actbio.2017.08.031.

[55] A. Torroni, C. Xiang, L. Witek, E.D. Rodriguez, P.G. Coelho, N. Gupta, Biocompatibility and degradation properties of WE43 Mg alloys with and without heat treatment: in vivo evaluation and comparison in a cranial bone sheep model, J. Cranio-Maxillo-Fac. Surg. 45 (2017) 2075–2083, https://doi.org/10.1016/j.jcms.2017.09.016.

[56] M.S. Dargusch, N. Balasubramani, J. Venezuela, S. Johnston, G. Wang, C. Lau, M. Bermingham, D. Kent, D.H. StJohn, Improved biodegradable magnesium alloys through advanced solidification processing, Scripta Mater. 177 (2020) 234–240, https://doi.org/10.1016/j.scriptamat.2019.10.028.

[57] Y. Chen, Z. Xu, C. Smith, J. Sankar, Recent advances on the development of magnesium alloys for biodegradable implants, Acta Biomater. 10 (2014) 4561–4573, https://doi.org/10.1016/j.actbio.2014.07.005.

[58] H.R.B. Rad, M.H. Idris, M.R.A. Kadir, S. Farahany, Microstructure analysis and corrosion behavior of biodegradable Mg-Ca implant alloys, Mater. Des. 33 (2012) 88–97, https://doi.org/10.1016/j.matdes.2011.06.057.

[59] W.C. Kim, J.G. Kim, J.Y. Lee, H.K. Seok, Influence of Ca on the corrosion properties of magnesium for biomaterials, Mater. Lett. 62 (2008) 4146–4148, https://doi.org/10.1016/j.matlet.2008.06.028.

[60] R.Q. Hou, C.Q. Ye, C.D. Chen, S.G. Dong, M.Q. Lv, S. Zhang, J.S. Pan, G.L. Song, C.J. Lin, Localized corrosion of binary Mg-Ca alloy in 0.9 wt% sodium chloride solution, Acta Metall. Sin. (Engl Lett). 29 (2016) 46–57, https://doi.org/10.1007/s40195-015-0361-2.

[61] A.D. Sudholz, N.T. Kirkland, R.G. Buchheit, N. Birbilis, Electrochemical properties of intermetallic phases and common impurity elements in magnesium alloys, Electrochem. Solid State Lett. 14 (2011) C5–C7, https://doi.org/10.1149/1.3523229.

[62] Y.S. Jeong, W.J. Kim, Enhancement of mechanical properties and corrosion resistance of Mg-Ca alloys through microstructural refinement by indirect extrusion, Corrosion Sci. 82 (2014) 392–403, https://doi.org/10.1016/j.corsci.2014.01.041.

[63] J.W. Seong, W.J. Kim, Development of biodegradable Mg-Ca alloy sheets with enhanced strength and corrosion properties through the refinement and uniform dispersion of the Mg2Ca phase by high-ratio differential speed rolling, Acta Biomater. 11 (2015) 531–542, https://doi.org/10.1016/j.actbio.2014.09.029.

[64] S.H. Cai, T. Lei, N.F. Li, F.F. Feng, Effects of Zn on microstructure, mechanical properties and corrosion behavior of Mg-Zn alloys, Mater. Sci. Eng. C 32 (2012) 2570–2577, https://doi.org/10.1016/j.msec.2012.07.042.

[65] Z.Y. Zou, J.H. Chen, H.G. Yan, B. Su, X.L. Gong, Microstructure, bio-corrosion behavior, and corrosion residual strength of high strain rate rolled Mg-4Zn alloy sheet, J. Mater. Eng. Perform. 25 (2016) 1974–1985, https://doi.org/10.1007/s11665-016-2041-4.

[66] A.F. Lotfabadi, H.R. Bakhsheshi-Rad, M.H. Idris, E. Hamzah, M. Kasiri-Asgarani, The role of solution heat treatment on corrosion and mechanical behaviour of Mg-Zn biodegradable alloys, Can. Metall. Q. 55 (2016) 53–64, https://doi.org/10.1179/1879139515Y.0000000031.

[67] Y.W. Song, E.H. Han, D.Y. Shan, C.D. Yim, B.S. You, The role of second phases in the corrosion behavior of Mg-5Zn alloy, Corrosion Sci. 60 (2012) 238–245, https://doi.org/10.1016/j.corsci.2012.03.030.

[68] Y.W. Song, E.H. Han, D.Y. Shan, C.D. Yim, B.S. You, The effect of Zn concentration on the corrosion behavior of Mg-xZn alloys, Corrosion Sci. 65 (2012) 322–330, https://doi.org/10.1016/j.corsci.2012.08.037.

[69] S.Y. Zhang, Y. Zheng, L.M. Zhang, Y.Z. Bi, J.Y. Li, J. Liu, Y.B. Yu, H.Q. Guo, Y. Li, In vitro and in vivo corrosion and histocompatibility of pure Mg and a Mg-6Zn alloy as urinary implants in rat model, Mater. Sci. Eng. C 68 (2016) 414–422, https://doi.org/10.1016/j.msec.2016.06.017.

[70] S.X. Zhang, X.N. Zhang, C.L. Zhao, J.A. Li, Y. Song, C.Y. Xie, H.R. Tao, Y. Zhang, Y.H. He, Y. Jiang, Y.J. Bian, Research on an Mg-Zn alloy as a degradable biomaterial, Acta Biomater. 6 (2010) 626–640, https://doi.org/10.1016/j.actbio.2009.06.028.

[71] Y. Yan, H.W. Cao, Y.J. Kang, K. Yu, T. Xiao, J. Luo, Y.W. Deng, H.J. Fang, H.Q. Xiong, Y.L. Dai, Effects of Zn concentration and heat treatment on the microstructure, mechanical properties and corrosion behavior of as-extruded Mg-Zn alloys produced by powder metallurgy, J. Alloys Compd. 693 (2017) 1277–1289, https://doi.org/10.1016/j.jallcom.2016.10.017.

[72] J. Hofstetter, M. Becker, E. Martinelli, A.M. Weinberg, B. Mingler, H. Kilian, S. Pogatscher, P.J. Uggowitzer, J.F. Löffler, High-strength low-alloy (HSLA) Mg–Zn–Ca alloys with excellent biodegradation performance, JOM 66 (2014) 566–572, https://doi.org/10.1007/s11837-014-0875-5.

[73] B.J. Kim, Y. Piao, M. Wufuer, W.-C. Son, T.H. Choi, Biocompatibility and efficiency of biodegradable magnesium-based plates and screws in the facial fracture model of beagles, J. Oral Maxillofac. Surg. 76 (2018), https://doi.org/10.1016/j.joms.2018.01.015, 1055.e1-1055.e9.

[74] N. Zhang, D. Zhao, N. Liu, Y. Wu, J. Yang, Y. Wang, H. Xie, Y. Ji, C. Zhou, J. Zhuang, Y. Wang, J. Yan, Assessment of the degradation rates and effectiveness of different coated Mg-Zn-Ca alloy scaffolds for in vivo repair of critical-size bone defects, J. Mater. Sci. Mater. Med. 29 (2018) 138, https://doi.org/10.1007/s10856-018-6145-2.

[75] L.B. Tong, M.Y. Zheng, X.S. Hu, K. Wu, S.W. Xu, S. Kamado, Y. Kojima, Influence of ECAP routes on microstructure and mechanical properties of Mg–Zn–Ca alloy, Mater. Sci. Eng. A 527 (2010) 4250–4256, https://doi.org/10.1016/j.msea.2010.03.062.

[76] S.M. Baek, H.K. Park, J.I. Yoon, J. Jung, J.H. Moon, S.G. Lee, J.H. Kim, T.S. Kim, S. Lee, N.J. Kim, H.S. Kim, Effect of secondary phase particles on the tensile behavior of Mg-Zn-Ca alloy, Mater. Sci. Eng. A 735 (2018) 288–294, https://doi.org/10.1016/j.msea.2018.08.050.

[77] Y. Du, D. Liu, Y. Ge, Effects of Ce addition on mechanical and corrosion properties of the as-extruded Mg-Zn-Ca alloy, J. Mater. Eng. Perform. 30 (2021) 488–496, https://doi.org/10.1007/s11665-020-05318-3.

[78] J. Hofstetter, S. Rüedi, I. Baumgartner, H. Kilian, B. Mingler, E. Povoden-Karadeniz, S. Pogatscher, P.J. Uggowitzer, J.F. Löffler, Processing and microstructure–property relations of high-strength low-alloy (HSLA) Mg–Zn–Ca alloys, Acta Mater. 98 (2015) 423–432, https://doi.org/10.1016/j.actamat.2015.07.021.

[79] Y.Z. Du, M.Y. Zheng, B.L. Jiang, Microstructure modification and resultant mechanical properties of Mg-6Zn-1.5Ca (wt%) alloy through hot extrusion, J. Mater. Res. 33 (2018) 1003–1010, https://doi.org/10.1557/jmr.2018.26.

[80] D. Liang, C.B. Cowley, The twin-roll strip casting of magnesium, JOM 56 (2004) 26–28, https://doi.org/10.1007/s11837-004-0122-6.

[81] R.V. Allen, D.R. East, T.J. Johnson, W.E. Borbidge, D. Liang, Magnesium alloy sheet produced by twin roll casting, Magnesium Technology 2001 (2001) 75–79, https://doi.org/10.1002/9781118805497.ch15.

[82] H. Watari, T. Haga, N. Koga, K. Davey, Feasibility study of twin roll casting process for magnesium alloys, J. Mater. Process. Technol. 192–193 (2007) 300–305, https://doi.org/10.1016/j.jmatprotec.2007.04.009.

[83] D.W. Kim, B.C. Suh, M.S. Shim, J.H. Bae, D.H. Kim, N.J. Kim, Texture evolution in Mg-Zn-Ca alloy sheets, Metall. Mater. Trans. 44 (2013) 2950–2961, https://doi.org/10.1007/s11661-013-1674-2.

[84] A. Javaid, F. Czerwinski, Progress in twin roll casting of magnesium alloys: a review, J. Magnes. Alloy (2020), https://doi.org/10.1016/j.jma.2020.10.003.

[85] C.W. Bale, E. Bélisle, P. Chartrand, S.A. Decterov, G. Eriksson, A.E. Gheribi, K. Hack, I.H. Jung, Y.B. Kang, J. Melançon, A.D. Pelton, S. Petersen, C. Robelin, J. Sangster, P. Spencer, M.A. Van Ende, FactSage thermochemical software and databases, 2010–2016, Calphad 54 (2016) 35–53, https://doi.org/10.1016/j.calphad.2016.05.002.

[86] H.R. Bakhsheshi-Rad, E. Hamzah, H.Y. Tok, M. Kasiri-Asgarani, S. Jabbarzare, M. Medraj, Microstructure, in vitro corrosion behavior and cytotoxicity of biodegradable Mg-Ca-Zn and Mg-Ca-Zn-Bi alloys, J. Mater. Eng. Perform. 26 (2017) 653–666, https://doi.org/10.1007/s11665-016-2499-0.

[87] E. Sitzmann, E.A. Marquis, Chemistry and morphology of β′ precipitates in an aged Mg-Nd-Y-Zr alloy, Phil. Mag. Lett. 95 (2015) 7–13, https://doi.org/10.1080/09500839.2014.995737.

[88] R.F. Dong, J.S. Li, H.C. Kou, B. Tang, K. Hua, S.B. Liu, Characteristics of a hot-rolled near beta titanium alloy Ti-7333, Mater. Char. 129 (2017) 135–142, https://doi.org/10.1016/j.matchar.2017.04.031.

[89] Y.N. Wang, J.C. Huang, Comparison of grain boundary sliding in fine grained Mg and Al alloys during superplastic deformation, Scripta Mater. 48 (2003) 1117–1122, https://doi.org/10.1016/S1359-6462(02)00615-2.

[90] K. Hantzsche, J. Bohlen, J. Wendt, K.U. Kainer, S.B. Yi, D. Letzig, Effect of rare earth additions on microstructure and texture development of magnesium alloy sheets, Scripta Mater. 63 (2010) 725–730, https://doi.org/10.1016/j.scriptamat.2009.12.033.

[91] J.J. Bhattacharyya, S.R. Agnew, G. Muralidharan, Texture enhancement during grain growth of magnesium alloy AZ31B, Acta Mater. 86 (2015) 80–94, https://doi.org/10.1016/j.actamat.2014.12.009.

[92] A. Incesu, A. Gungor, Mechanical properties and biodegradability of Mg–Zn–Ca alloys: homogenization heat treatment and hot rolling, J. Mater. Sci. Mater. Med. 31 (2020) 123, https://doi.org/10.1007/s10856-020-06468-5.

[93] H. Bai, X. He, P. Ding, D. liu, M. Chen, Fabrication, microstructure, and properties of a biodegradable Mg-Zn-Ca clip, J. Biomed. Mater. Res. B Appl. Biomater. 107 (2019) 1741–1749, https://doi.org/10.1002/jbm.b.34267.

[94] H.-x. Li, S.-k. Qin, Y.-z. Ma, J. Wang, Y.-j. Liu, J.-s. Zhang, Effects of Zn content on the microstructure and the mechanical and corrosion properties of as-cast low-alloyed Mg–Zn–Ca alloys, Int. J. Miner. Metall. Mater. 25 (2018) 800–809, https://doi.org/10.1007/s12613-018-1628-1.

[95] F. Witte, V. Kaese, H. Haferkamp, E. Switzer, A. Meyer-Lindenberg, C.J. Wirth, H. Windhagen, In vivo corrosion of four magnesium alloys and the associated bone response, Biomaterials 26 (2005) 3557–3563, https://doi.org/10.1016/j.biomaterials.2004.09.049.

[96] N.I. Zainal Abidin, B. Rolfe, H. Owen, J. Malisano, D. Martin, J. Hofstetter, P.J. Uggowitzer, A. Atrens, The in vivo and in vitro corrosion of high-purity

magnesium and magnesium alloys WZ21 and AZ91, Corrosion Sci. 75 (2013) 354–366, https://doi.org/10.1016/j.corsci.2013.06.019.

[97] G. Song, Control of biodegradation of biocompatable magnesium alloys, Corrosion Sci. 49 (2007) 1696–1701, https://doi.org/10.1016/j.corsci.2007.01.001.

[98] J. Kuhlmann, I. Bartsch, E. Willbold, S. Schuchardt, O. Holz, N. Hort, D. Höche, W.R. Heineman, F. Witte, Fast escape of hydrogen from gas cavities around corroding magnesium implants, Acta Biomater. 9 (2013) 8714–8721, https://doi.org/10.1016/j.actbio.2012.10.008.

[99] E.D. McBride, Absorbable metal in bone surgery: a Further report on the use of Magnesium Alloys, JAMA Surg 111 (1938) 2464–2467, https://doi.org/10.1001/jama.1938.02790530018007.

[100] Y.K. Kim, K.B. Lee, S.Y. Kim, K. Bode, Y.S. Jang, T.Y. Kwon, M.H. Jeon, M.H. Lee, Gas formation and biological effects of biodegradable magnesium in a preclinical and clinical observation, Sci. Technol. Adv. Mater. 19 (2018) 324–335, https://doi.org/10.1080/14686996.2018.1451717.

[101] F. Amerstorfer, S.F. Fischerauer, L. Fischer, J. Eichler, J. Draxler, A. Zitek, M. Meischel, E. Martinelli, T. Kraus, S. Hann, S.E. Stanzl-Tschegg, P. J. Uggowitzer, J.F. Loffler, A.M. Weinberg, T. Prohaska, Long-term in vivo degradation behavior and near-implant distribution of resorbed elements for magnesium alloys WZ21 and ZX50, Acta Biomater. 42 (2016) 440–450, https://doi.org/10.1016/j.actbio.2016.06.025.

[102] Y. Kim, K.-B. Lee, S.y. Kim, K. Bode, Y.-S. Jang, T.-Y. Kwon, M. Jeon, M.H. Lee, Gas formation and biological effects of biodegradable magnesium in a preclinical and clinical observation, Sci. Technol. Adv. Mater. 19 (2018) 1–26, https://doi.org/10.1080/14686996.2018.1451717.

[103] L. Elkaiam, O. Hakimi, G. Yosafovich-Doitch, S. Ovadia, E. Aghion, Vivo evaluation of Mg–5%Zn–2%Nd alloy as an innovative biodegradable implant material, Ann. Biomed. Eng. 48 (2020) 380–392, https://doi.org/10.1007/s10439-019-02355-5.

[104] D. Noviana, D. Paramitha, M.F. Ulum, H. Hermawan, The effect of hydrogen gas evolution of magnesium implant on the postimplantation mortality of rats, J. Orthop. Translat. 5 (2016) 9–15, https://doi.org/10.1016/j.jot.2015.08.003.

[105] J.M. Anderson, A. Rodriguez, D.T. Chang, Foreign body reaction to biomaterials, Semin. Immunol. 20 (2008) 86–100, https://doi.org/10.1016/j.smim.2007.11.004.

[106] T. Urade, T. Yoshida, N. Ikeo, K. Naka, M. Kido, H. Toyama, K. Ueno, M. Tanaka, T. Mukai, T. Fukumoto, Novel biodegradable magnesium alloy clips compared with titanium clips for hepatectomy in a rat model, BMC Surg. 19 (2019) 130, https://doi.org/10.1186/s12893-019-0600-y.

[107] P. Ding, Y. Liu, X. He, D. Liu, M. Chen, In vitro and in vivo biocompatibility of Mg–Zn–Ca alloy operative clip, Bioact. Mater. 4 (2019) 236–244, https://doi.org/10.1016/j.bioactmat.2019.07.002.

[108] G. Mao, X. Jin, J. Sun, X. Han, M. Zeng, Y. Qiu, W. Bian, Microalloying design of biodegradable Mg–2Zn–0.05Ca promises improved bone-implant applications, ACS Biomater. Sci. Eng. 7 (2021) 2755–2766, https://doi.org/10.1021/acsbiomaterials.1c00218.

[109] C. Zhang, J. Lin, N.-Y.T. Nguyen, Y. Guo, C. Xu, C. Seo, E. Villafana, H. Jimenez, Y. Chai, R. Guan, H. Liu, Antimicrobial bioresorbable Mg–Zn–Ca alloy for bone repair in a comparison study with Mg–Zn–Sr alloy and pure Mg, ACS Biomater. Sci. Eng. 6 (2020) 517–538, https://doi.org/10.1021/acsbiomaterials.9b00903.

[110] J. Gong, M. Sun, S. Wang, J. He, Y. Wang, Y. Qian, Y. Liu, L. Dong, L. Ma, K. Cheng, W. Weng, M. Yu, Y.S. Zhang, H. Wang, Surface modification by divalent main-group-elemental ions for improved bone remodeling to instruct implant biofabrication, ACS Biomater. Sci. Eng. 5 (2019) 3311–3324, https://doi.org/10.1021/acsbiomaterials.9b00270.

[111] Y. Wang, Z. Geng, Y. Huang, Z. Jia, Z. Cui, Z. Li, S. Wu, Y. Liang, S. Zhu, X. Yang, W.W. Lu, Unraveling the osteogenesis of magnesium by the activity of osteoblasts in vitro, J. Mater. Chem. B. 6 (2018) 6615–6621, https://doi.org/10.1039/C8TB01746H.